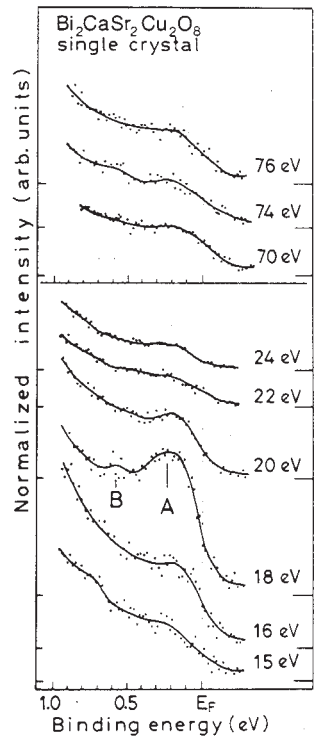

Fig. 2 Photoemission spectra of single-crystal $Bi_2CaSr_2Cu_2O_8$ in the vicinity of the Fermi level measured with photon energies near the O 2*s* (lower) and Cu 3*p* (upper) core thresholds in the normal-emission arrangement. The photon energy used is indicated on each spectrum. The intensity of photoemission is normalized to the incident-photon flux, independently for the O 2*s* and Cu 3*p* regions.

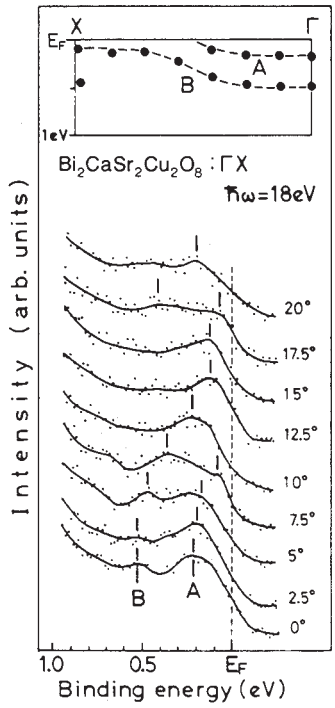

Fig. 3 Angle-resolved photoemission spectra of single-crystal $Bi_2CaSr_2Cu_2O_8$ measured in the high-symmetry direction ΓX for $\hbar\omega = 18$ eV. Inset: band structure determined from angle-resolved photoemission.

Figure 2 shows the photon-energy dependence of the spectrum in the vicinity of the Fermi level for the energy regions near the O 2*s* and Cu 3*p* core thresholds. The spectra are normalized to the incident-photon flux. The photoemission intensity, and hence the density of states, at the Fermi level (band A) exhibits enhancement at the O 2*s* core threshold ($\hbar\omega = 18$ eV) but no such enhancement is observed at the Cu 3*p* core threshold ($\hbar\omega = 74$ eV), indicating, as explained below, that the electronic states at the Fermi level in $Bi_2CaSr_2Cu_2O_8$ have a dominant O 2*p* nature.

Figure 3 shows angle-resolved photoemission spectra in the vicinity of the Fermi level measured in a high-symmetry direction in momentum space (ΓX) for $\hbar\omega = 18$ eV. The inset shows the band structure implied by the spectra. Comparison with a band structure calculation including the higher-binding-energy region has been described elsewhere[7]. Figure 3 shows that there are two bands, with a substantial energy dispersion of 0.2–0.5 eV, in the vicinity of the Fermi level and that one of them crosses the Fermi level midway between the Γ point and the Brillouin-zone boundary. This is clear evidence for the existence of a Fermi-liquid state in the high-T_c superconductor and is consistent with the recently discovered BSC-like enhancement of the enriched ^{17}O nuclear relaxation rate below T_c (ref. 8). Both experiments indicate that doped holes, residing mainly on the oxygen site owing to the strong on-site Coulomb repulsion at the copper site, behave like a Fermi liquid. The resonant effect observed at the O 2*s* core threshold (Fig. 2) is due to 2*s*–2*p* absorption, implying that there is an empty O 2*p* state just above the Fermi level. This supports recent results of electron-energy-loss-spectroscopy (EELS)[9], in which a small absorption peak just above the O 1*s* absorption edge was ascribed to empty O 2*p* states.

Thus, the present experimental results provide a clear picture of the electronic structure of the high-T_c superconductor, which consists of two major features: a Fermi-liquid state with predominantly O 2*p* character and strongly localized states away from the Fermi level with both Cu 3*d* and O 2*p* character. Superconductivity could be driven by Cooper-pairing of the O 2*p* holes in the Fermi-liquid state.

We thank Professors M. Tachiki and Y. Kuramoto for useful discussion. This work was supported by a grant from the Ministry of Education, Japan.

Receieved 15 July; accepted 29 July 1988.

1. Takahashi, T. *et al. Phys. Rev.* B36, 5686–5689 (1987).
2. Shen, Z. *et al Phys Rev.* B36, 8414–8428 (1987).
3. Katayama-Yoshida, H., Ikabe, Y., Takahashi, T. & Hosoya, S. *Jap. J. appl. Phys.* (submitted).
4. Hybertsen, M. S. & Mattheiss, L. F. *Phys. Rev. Lett.* **60**, 1661–1664 (1988).
5. Krakauer, H. & Pickett, W. E. *Phys. Rev. Lett.* **60**, 1665–1667 (1988).
6. Massidda, S., Yu, J. & Freeman, A. J. *Physica* C52, 251–258 (1988).
7. Takahashi, T. *et al. Phys. Rev. Lett.* (sumitted).
8. Kitaoka, Y. *et al. Nature* (submitted).
9. Nücker, N., Fink, J., Fuggle, J. C., Durham, P. J. & Temmerman, W. M. *Phys. Rev.* B37, 5158–5163 (1988).

Controlled crystallization of $CaCO_3$ under stearic acid monolayers

Stephen Mann*, Brigid R. Heywood*, Sundara Rajam* & J. Derek Birchall†

* School of Chemistry, University of Bath, Bath BA2 7AY, UK
† ICI Advanced Materials, Runcorn, Cheshire WA7 4QE, UK

A fundamental concept in the study of biomineralization concerns the molecular recognition of inorganic materials at organized organic macromolecular substrates[1]. Here we investigate this concept through the use of stearic acid monolayers in the controlled crystallization of $CaCO_3$ from supersaturated solutions. Whereas crystallization in the absence of a monolayer results in rhombohedral calcite crystals, the presence of an organized monolayer gives

Table 1 XRD values

Experimental		Theoretical	
Trough	Control	Calcite	Vaterite
4.241			4.245
	3.843	3.852	
3.576			3.577
3.290			3.296
	3.030	3.030	
	2.831	2.834	
2.726			2.735
	2.262	2.284	
2.202			2.219
2.112			2.122
	2.079	2.094	
2.060			2.065
	1.901	1.907	
	1.865	1.872	
1.857			1.857
1.820			1.825
1.645			1.648
	1.619	1.604	
	1.591	1.582	
1.534			1.544
1.471			1.477
	1.468	1.506	
	1.437	1.440	
	1.417	1.416	
1.358			1.351
	1.334	1.336	
1.308			1.331
1.283			1.286
	1.175	1.177	
	1.141	1.141	

All analyses were performed on a Phillips powder diffractometer—Cu Kα radiation ($\lambda = 1.5405$ Å).

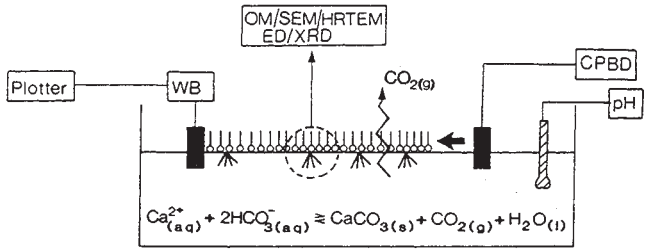

Fig. 1 Experimental procedure for the growth of $CaCO_3$ crystals under stearic acid monolayers. Monolayer films of stearic acid ($CH_3(CH_2)_{16}COOH$) were deposited on supersaturated calcium bicarbonate solutions freshly prepared using the method of Kitano[10]. A value of $S = 10^3$, where S is a measure of the maximum attainable supersaturation (namely that generated under conditions of instantaneous outgassing of all the CO_2) was estimated by titrimetric analysis. The experimental pH (5.8–6.0) was above the pK_a (5.1) of stearic acid. Films were either uncompressed or compressed to liquid (20 mN m^{-1}) or solid (40 mN m^{-1}) phases and then left undisturbed for periods up to 16 h, during which crystal growth occurred by CO_2 outgassing. Crystals were collected from the monolayer surface at various times for structural and morphological analysis. Bulk samples for X-ray diffraction (XRD) were obtained by sweeping the surface with the barrier and collecting the aggregated crystals on glass slides. Crystals for optical microscopy (OM) were viewed *in situ* or on glass slides dipped through the films. Samples for scanning electron microscopy (SEM) were obtained by carefully touching the film surface with stainless steel stubs so that crystals were transferred by surface tension with only minimal disruption of their crystallographic organization. Crystals grown for 0–60 min were collected by gently dipping nitrocellulose-covered carbon-coated copper electron microscope grids once through the monolayer and were studied by high resolution transmission electron microscopy (HRTEM) and electron diffraction (ED). WB, Wilhelmy balance; CPBD, constant perimeter barrier device.

rise to oriented vaterite formation. The vaterite nuclei are aligned with their (0001) face parallel to the plane of the organic substrate and develop initially in the form of disk-shaped single crystals. The degree of compression of the monolayer dictates the homogeneity of vaterite nucleation. In particular, partially compressed films are optimal for controlled crystallization, suggesting that the mobility of organic surfaces may be of general importance. Our results can be explained by electrostatic and stereochemical interactions at the inorganic–organic interface and these observations support current theories of biomineralization, as well as being of potential significance in the crystal engineering of microscopic inorganic assemblies[2].

The influence of structured organic surfaces on the oriented overgrowth of inorganic minerals is a fundamental aspect of biomineralization. Addadi and co-workers[3,4] have studied the effect of β-pleated sheet proteins on the crystallization of calcite and showed that a cooperative effect arising from electrostatic, structural and stereochemical requirements gave rise to oriented calcite nucleation. Mann *et al.*[5] used organized phospholipid vesicles to control the structure of iron oxide phases formed from aqueous solution. Recently, Landau *et al.*[6,7] showed that oriented growth of glycine and, to a lesser extent, NaCl takes place at the air/water interface of Langmuir monolayers. In this paper, we describe the role of Langmuir monolayers in determining the structure, morphology and crystallographic orientation of $CaCO_3$ crystals formed from supersaturated solutions.

The experimental procedure for growing calcium carbonate crystals under stearic acid monolayers is shown diagrammatically in Fig. 1. In the absence of a monolayer, rhombohedral calcite crystals were formed (Table 1) at the surface, sides and bottom of the trough. Crystal growth at the solution surface was favoured as a result of continual CO_2 outgassing and the local supersaturation levels remained low, as shown by the absence of kinetically stabilized polymorphs such as aragonite and vaterite. In contrast, in the presence of fully and partially compressed monolayers, crystallization was confined to the organic surface and the crystal structure was exclusively vaterite (Table 1). The mature vaterite crystals had a narrow particle-size distribution (mean 75 μm, $\sigma = 10$ μm) and exhibited a complex pseudo-hexagonal floret morphology (Fig. 2*A*). The early crystals developed anisotropically along the organic interface in the form of lens-shaped disks (Fig. 2*B*). Disks of diameter ~3 μm were subsequently transformed into the floret habit by radial outgrowth into bulk solution. *In situ* optical microscopical investigations combined with scanning electron microscope observations indicated that the ventral surface of each disk was apposed to the monolayer with their radial axis normal to the plane of the interface. Electron diffraction patterns were recorded from individual disks and showed that the particles were single crystals of vaterite and that the radial axis corresponded to the crystallographic [0001] (c) axis (Fig. 2*C* and *D*). Viewed from the side, the disks were lens-shaped and gave diffraction patterns corresponding to either the crystallographic a ([1210]) axes or the [1010] axis (Fig. 2*E* and *F*). These results indicate that the crystallographic c and a axes were oriented perpendicular and parallel to the monolayer surface respectively and that nucleation of the disks occurred on the (0001) face of vaterite.

Compression isotherms (data not shown) for stearic acid on pure water gave a value for the limiting area per molecule of 22 Å^2. Films compressed on calcium-containing solutions gave a slightly expanded limiting area of 24 Å^2 and a characteristic reduction in the surface pressure during the liquid-to-solid phase transformation[8]. These results indicated that Ca-binding to the carboxylate headgroups preceeded nucleation at the monolayer surface. The formation of a Stern layer of Ca counterions favours

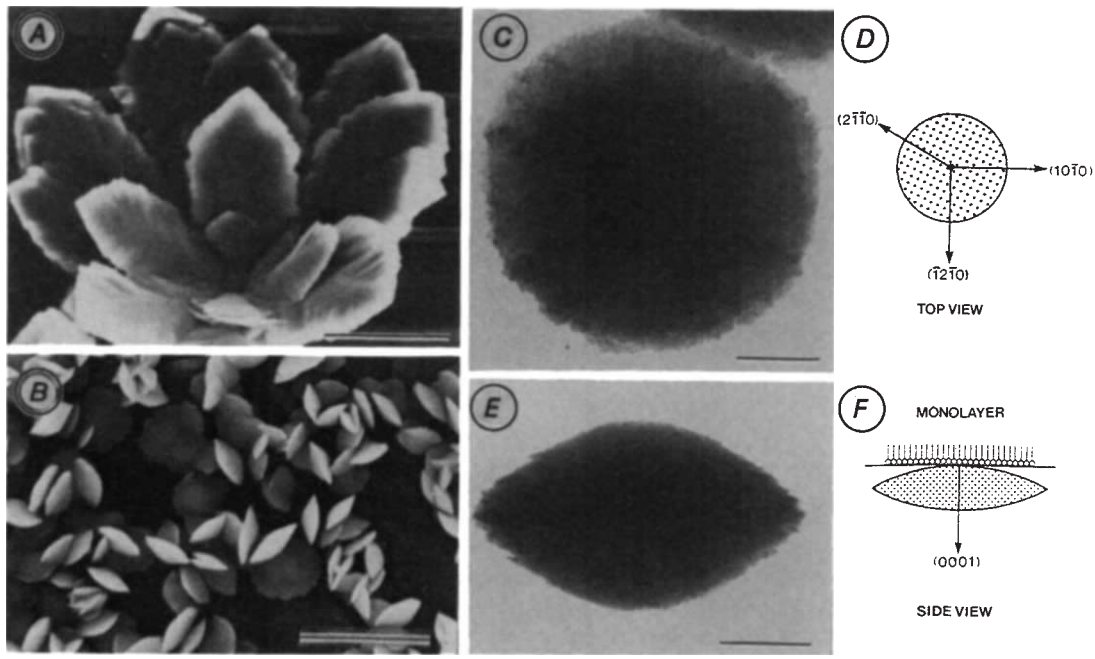

Fig. 2 *A*, SEM of mature vaterite floret. The florets exhibit a complex crystalline pseudo-hexagonal morphology. Plate-like outgrowths radiate from a central disk-shaped core. Scale bar, 10 μm. *B*, SEM of vaterite disks. The early crystals develop anisotropically along the monolayer in the form of lens-shaped disks. Radial outgrowth into the solution subphase transforms the disks into the mature floral habit. Scale bar, 5.0 μm. *C*, TEM of vaterite disk, top view. Scale bar, 0.5 μm. *E*, TEM of vaterite disk, side view. Scale bar, 0.5 μm. *D*, *F*, Relationship between the morphology of the growing crystals, their crystallographic orientation and the stearic acid monolayer. The crystallographic axes *c* (0001) and *a* (2$\bar{1}\bar{1}$0; $\bar{1}$2$\bar{1}$0; 10$\bar{1}$0) were determined from electron diffraction patterns of the disks.

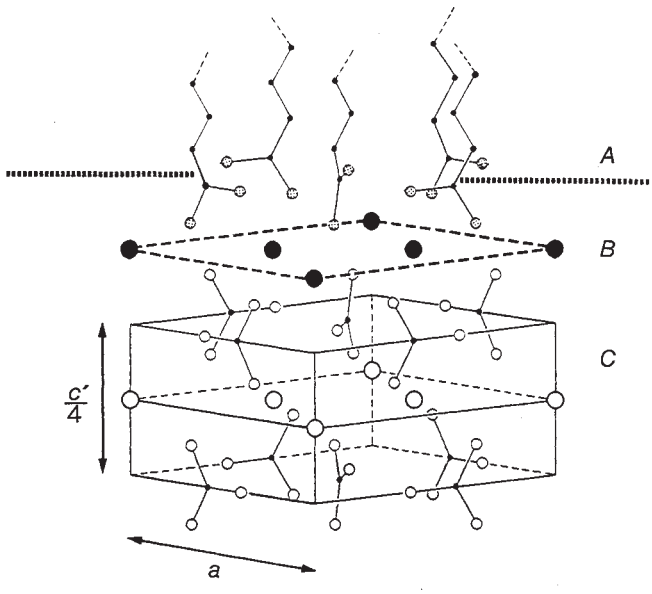

Fig. 3 Proposed organization of the interface between stearic acid monolayers and nascent vaterite nuclei. *A*, Monolayer surface showing carboxylates aligned perpendicular to the air/water interface; the minimum inter-headgroup spacing for stearic acid is ~4.6 Å; *B*, Stern layer of headgroup-bound Ca^{2+} ions; the uni-charged layer is electrostatically equivalent to the (0001) face of vaterite, although the Ca–Ca distances are different; *C*, vaterite sub-cell showing the stereochemical arrangement of carbonates perpendicular to the (0001) face; $c'/4 = 4.25$ Å, $a = 7.15$ Å. (●, ○) Ca atoms, Stern layer and vaterite cells respectively; (○, ⊜) O atoms, vaterite cell and carboxylates respectively; (●) C atoms.

the oriented nucleation of crystal faces consisting of only Ca atoms and the (0001) face of vaterite fits this criterion (Fig. 3). Charge accumulation, however, cannot account for the structural selectivity of vaterite, as the (0001) face of calcite is also uni-charged. The trigonal planar carbonate anions are oriented parallel to the (0001) face of calcite, whereas in vaterite they are aligned perpendicularly, and this latter arrangement is equivalent to the orientation of the carboxylate headgroups with respect to the Ca-bound Stern layer. Thus, the stereochemical arrangement of the carboxylates in conjunction with Ca binding generates a two-layer subunit cell motif of the vaterite structure, rather than calcite (Fig. 3). Subsequent addition of carbonate from solution will be similarly stereochemically directed extending the vaterite motif towards a stable nucleus.

We emphasize that the mechanism proposed above does not involve the epitaxial matching of lattice dimensions in the (0001) face and headgroup spacings in the compressed monolayer film. The inter-headgroup spacing on the fully compressed monolayer is ~4.6 Å, compared with a Ca–Ca distance of 4.13 Å in vaterite (4.96 Å in calcite). Thus the Stern layer shown in Fig. 3 is expanded compared with the layer of Ca atoms in the vaterite unit cell. This point highlights the importance of stereochemical and electrostatic matching because these factors can override the structural mismatch at the interface. Moreover, if geometric matching was a fundamental property of the system, we would expect calcite to be favoured over vaterite because the former has Ca–Ca distances that can be spanned by the carboxylate headgroups, for example in a partially compressed film.

Whereas fully compressed monolayers promoted rapid vaterite nucleation indiscriminately across the entire interface, resulting in small disks with a wide distribution of diameters (mean 1.32 μm, $\sigma = 0.47$ μm, $t = 35$ min), and nucleation on uncompressed films was slow and comparable with calcite nucleation from bulk solution, nucleation on partially compressed monolayers was intermediate in rate, as shown by a

narrow size distribution of relatively large (mean 2.23 μm, σ = 0.18 μm, t = 35 min) but fewer vaterite disks. We propose that the rate of nucleation on liquid-phase monolayers is optimal because it requires the Ca-induced local ordering of stearate molecules into a configuration tailored for nucleation. Once formed, these sites are autocatalytic and successfully compete against the formation of new nucleation centres on the monolayer such that nucleation is confined to a limited number of discrete sites across the organic surface.

Finally, we note that organized macromolecular surfaces such as β-pleated sheet proteins and phospholipid membranes are components of many biological systems involving calcification[9]. With regard to the above observations, optimal control of biomineralization could be achieved on surfaces that are activated for nucleation through specific conformational changes induced by ion-binding, rather than on surfaces sterically predisposed and hence highly catalytic for nucleation. A mechanism of this type would be synergic as the coordination of specific ions present under supersaturated concentrations induces local interfacial modifications that, in turn, direct the flow of additional ions to the site and the subsequent development of the inorganic nucleus.

We thank Dr N. H. C. Sparks for assistance with scanning electron microscopy. The work was supported in part by SERC. S.R. is in receipt of a SERC/CASE studentship with ICI plc.

Received 27 April; accepted 19 July 1988.

1. Mann, S. *Nature* **332**, 119-124 (1988).
2. Calvert, P. D. & Mann, S. *J. Mater. Sci.* (in the press).
3. Addadi, L. & Weiner, S. *Proc. natn. Acad. Sci. U.S.A.* **82**, 4110-4114 (1985).
4. Addadi, L., Moradian, J., Shay, E., Maroudas, N. G. & Weiner, S. *Proc. natn. Acad. Sci. U.S.A.* **84**, 2732-2736 (1987).
5. Mann, S., Hannington, J. P. & Williams, R. J. P. *Nature* **324**, 565-567 (1986).
6. Landau, E. M., Levanon, M., Leiserowtiz, L., Lahav, M. & Sagiv, J. *Nature* **318**, 353-356 (1985).
7. Landau, E. M. *et al. Molec. Cryst. liq. Cryst.* **134**, 323-335 (1986).
8. Gordziel, M. J., Flanagan, D. R. & Swarbrick, J. *J. Colloid. Interface Sci.* **86**, 178-184 (1981).
9. Weiner, S. *CRC Crit. Rev. Biochem.* **20**, 365-408 (1986).
10. Kitano, Y. *Bull. chem. Soc. Japan.* **12**, 1980-1985 (1962).

Observed velocity fluctuations on a major Antarctic ice stream

S. N. Stephenson* & R. A. Bindschadler†

* Science Applications Research, 4400 Forbes Boulevard, Lanham, Maryland 20706, USA
† Code 671, NASA/Goddard Space Flight Center, Greenbelt, Maryland 20771, USA

Most of the Antarctic ice sheet is drained by systems comprising an area of slow sheet flow which converges into a much faster valley glacier or ice stream. On reaching the coast, this ice then either enters an ice shelf confined by embayments and ice rises, or calves off into the ocean. The higher speed of ice streams enables them to respond to changes in their environment faster than the slower ice sheet. In the West Antarctic, where the ice sheet moves across bedrock well below sea level, the ice streams have the potential to rapidly increase or decrease the ice discharge into the sea[1]. The timescale for these changes has been placed at a few hundred years. If this is true, then changes should be detectable by careful measurements on a decadal timescale. By comparing recent ice velocity measurements with those collected ten years ago, we establish that the ice in the mouth of Ice Stream B has decelerated by ~20%. We discuss the possible causes of this deceleration on the basis of our knowledge of the current regional dynamics, and the possible ramifications of this deceleration on future ice stream behaviour.

Doppler satellite tracking methods were used to obtain ice velocities during the Ross Ice Shelf Geophysical and Glaciological Survey (RIGGS) between 1972 and 1974, and then again during the current Siple Coast Program (SCP) begun in 1983. Both programs collected data on a 100-km section of ice extending from the ice shelf just upstream of Crary Ice Rise on to the ice plain of Ice Stream B (Fig. 1). The term ice plain refers to the area immediately upstream of the grounding line which has shallow surface slope similar to an ice shelf, and experiences only a very small amount of bed friction[2]. Velocities were measured by determining the position of markers twice, taking the velocity as being the distance between positions divided by the time interval between measurements. The velocities are presented in Table 1.

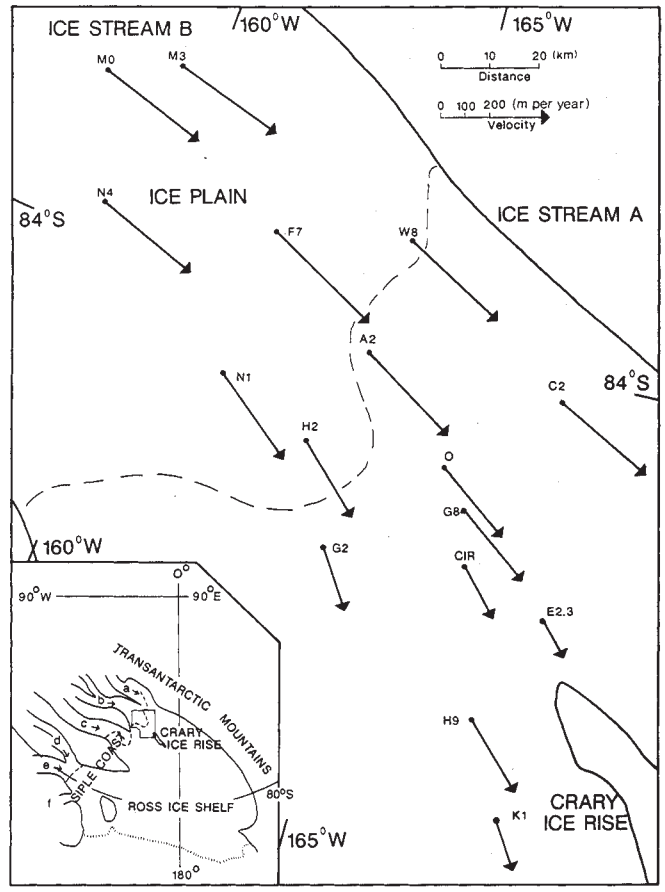

Fig. 1 Ice velocities upstream of Crary Ice Rise and on the ice plain of Ice Stream B. The thick continuous lines indicate ice-stream boundaries (after ref. 8, with modifications). The broken line indicates the grounding line. The inset shows the relative positions of the ice streams feeding the Ross Ice Shelf.

The velocities during RIGGS were determined using precise satellite ephemerides, but data from only a few (~5) satellite passes. The accuracy of these measurements is discussed by Thomas *et al.*[3]. They do not give details of the individual determinations at each site, but estimate an error of 15 m per yr for all the velocities. They regard this error as a conservative estimate because a systematic part of the positional error does not contribute to the velocity.

The velocities determined during SCP used the broadcast ephemeris and a simple model to compensate for tropospheric refraction. Data from a minimum of 5 and a maximum of 28 passes were used in the velocity determinations which are compared with RIGGS data. MacDonald and Whillans[4] estimate that the error in the isolated point-position determination is near 30 m, but they do not estimate how much of this error is systematic with position. Any systematic error would not contribute to the error in velocity. Four velocities at nearby stations,